Determination of the spectral variation origin in high-order harmonic generation in noble gases

V. E. Nefedova,[1,2] M. F. Ciappina,[1,*] O. Finke,[1,2] M. Albrecht,[1,2] J. Vábek,[1,2,3] M. Kozlová,[1,4]
N. Suárez,[5] E. Pisanty,[5] M. Lewenstein,[5,6] and J. Nejdl[1,4,†]

[1]*Institute of Physics of the ASCR, ELI-Beamlines project, Na Slovance 2, 182 21 Prague, Czech Republic*
[2]*Faculty of Nuclear Sciences and Physical Engineering CTU, Brehova 7, 115 19 Prague 1, Czech Republic*
[3]*Centre Lasers Intenses et Applications CNRS-CEA, Université de Bordeaux, 351 Cours de la Libération, Talence F-33405, France*
[4]*Institute of Plasma Physics ASCR, Za Slovankou 3, 182 00 Prague 8, Czech Republic*
[5]*ICFO - Institut de Ciencies Fotoniques, The Barcelona Institute of Science and Technology, 08860 Castelldefels (Barcelona), Spain*
[6]*ICREA, Pg. Lluís Companys 23, 08010 Barcelona, Spain*

One key parameter in the high-order harmonic generation (HHG) phenomenon is the exact frequency of the generated harmonic field. Its deviation from perfect harmonics of the laser frequency can be explained by considering (i) the single-atom laser-matter interaction and (ii) the spectral changes of the driving laser. In this work, we perform an experimental and theoretical study of the causes that generate spectral changes in the HHG radiation. We measured the driving-laser spectral shift after HHG in a long medium by using a correction factor to take into account the multiple possible HHG initiation distances along the laser path. We separate out the contribution of laser spectral shift from the resultant high-harmonic spectral shift in order to elucidate the microscopic effect of spectral shift in HHG. Therefore, in some cases we are able to identify the dominant electron trajectory from the experimental data. Our investigations lead to valuable conclusions about the atomic dipole phase contribution to a high-harmonic spectral shift. We demonstrate that the significant contribution of a long electron path leads to a high-harmonic shift, which differs from that expected from the driving laser. Moreover, we assess the origin of the high-order harmonics spectral broadening and provide an explanation for the narrowest high-harmonic spectral width in our experiment.

DOI: 10.1103/PhysRevA.98.033414

I. INTRODUCTION

Development of coherent light sources in the extreme ultraviolet (XUV) spectral domain is of very high importance because it allows researchers to carry out wavelength-limited imaging, observation, and potentially control of various physical, biological, and chemical phenomena at their natural spatial, nanometric, and temporal (subfemtosecond) scales. The highly nonlinear interaction of intense femtosecond laser pulses with matter leads to the generation of harmonics of the driving-laser light up to very high orders. This phenomenon, so-called high-order harmonic generation (HHG), became the flagship source of short-wavelength coherent radiation [1]. A major benefit of sources based on HHG lies in their compactness and low cost, enabling wide availability for researchers. Besides its high degree of coherence, HHG radiation exhibits collimated beams [2] with a Gaussian-like transverse energy distribution and a nearly-diffraction-limited wavefront [3], allowing for efficient focusing of the light onto samples. Furthermore, these properties facilitate the analysis of the source features and allow engineering of their temporal and spatial characteristics. Likewise, the polarization state of the emitted radiation can be controlled to a high degree [4] (for a recent review see, e.g., Ref. [5]).

During the last few decades significant efforts were put into the understanding of the main mechanisms driving the HHG process. From a spectral point of view, HHG has been demonstrated over a very wide range of wavelengths, spanning from tens of nanometers to a few angstroms [6]. Additionally, the intrinsic nature of the HHG phenomenon allows the generation of ultrashort pulses; indeed, it was shown that these sources can reach the attosecond (as) temporal range (1 as = 10^{-18} s) [7,8], allowing an insight into the ultrafast electron dynamics inside matter [9]. Other possible applications of these ultrashort coherent XUV sources include following transient elementary processes [10], scrutinizing ultrafast magnetization effects [11] and monitoring molecular processes in real time [12]. Depending on the technology of the laser driver, HHG sources can be operated in a single-shot mode or at very high repetition rates. The former makes it possible to conduct pump-probe experiments with samples that are nonrenewable [13,14], while the latter favors studies (such as photoelectron spectroscopy) where accumulation of a low intensity signal is required.

It is therefore important to find tools able to control the frequency of the XUV ultrashort pulses generated through HHG. The current contribution provides a detailed study of the HHG frequency variation, which could be advantageously used for time-resolved ultrafast experiments.

At a single-atom level, the HHG process can be easily explained by a semiclassical description; namely, by invoking what is known as the "three-step model": first, an atom is

---

*marcelo.ciappina@eli-beams.eu
†jaroslav.nejdl@eli-beams.eu

ionized by the strong electric field of the laser, so the electron wave packet can leave the atomic potential via tunneling; next, the free electron is accelerated by the laser field, defining the second stage of the sequence, and, finally, when the laser electric field reverses sign, the electron can recombine with its parent ion, emitting the energy obtained during its journey in the laser-dressed continuum in the form of XUV radiation [15–17].

From a macroscopic viewpoint, the individual fields emitted by atoms located at different positions in the propagation direction need to be in phase, so that their respective electric fields can add up constructively, allowing the growth of the XUV intensity. The wave-vector mismatch, defined as $\Delta k = q k_1 - k_q$, where q is the harmonic order and k_1 and k_q are the wave vectors of the fundamental driving field and the one of the qth harmonic order, respectively, consists of contributions from plasma Δk_p and neutral atoms Δk_n. There is also a mismatch due to the Gouy phase shift Δk_G and the atomic dipole Δk_d, which originates from the intensity gradient of the incident beam and depends on the electron trajectory (short or long) responsible for the emission. One of the areas of intense research encompasses the development and implementation of configurations with larger interaction lengths—the length over which the two fields are phase matched, known as the coherence length and defined as $L_{\mathrm{coh}} = \frac{\pi}{\Delta k}$. The condition, which minimizes the wave-vector mismatch and turns Δk close to zero, is called phase matching [18,19].

Considerable attempts have been made to obtain control of the different quantum path contributions with a low driving-laser intensity [20]. In this work, we use a method that allows us to determine the origin of the spectral variation of individual harmonics when the driving-laser intensity increases. We perform a real-time monitoring of the driving laser's spectral properties, which provides a beneficial approach for its control during the HHG process. The postinteraction infrared (IR) spectra are recorded on-axis, simultaneously with the HHG spectrum. The data obtained are then used to discriminate the contributions due to the driving-laser wavelength shift from the intrinsic contributions that are inherent to every HHG phenomenon at the single-atom level.

This paper is organized as follows: in the next section, Sec. II, we describe the experimental setup. Section III is devoted to the theoretical framework, including all the sources for the phase variation of HHG and Sec. IV is focused on the results and discussion. Here we include the determination of the intensity-dependent quantum-path phase coefficients and a comparison between our theoretical predictions with the experimental data. Finally, in Sec. V, we summarize the main ideas and present our conclusions.

II. EXPERIMENTAL SETUP

The HHG experiment was carried out by using a 10 Hz Ti:sapphire laser system, wavelength centered at about $\lambda_{\mathrm{IR}} = 810$ nm with a pulse energy from 50 to 125 mJ. Additionally, the pulse duration was estimated to be 50 fs full width at half maximum (FWHM) of intensity by using an autocorrelation technique. The laser beam was loosely focused by a spherical mirror with a focal length of $f = 5$ m into a gas cell filled with a noble gas (argon, neon, or helium), as shown in Fig. 1.

The incident laser beam diameter D (and thus the transferred energy E) is varied by changing the diameter of an iris aperture, providing a range of $F_\#$ ($F_\# = f/D$) from 150 to 400. The fundamental IR beam was focused into the gas cell to produce high-order harmonics, which follow the laser propagation direction. A thin metallic transmission filter was placed about 5 m away from the HHG source at the entrance of the diagnostics chamber in order to reject the IR radiation. A flat-field spectrometer, with a reflective concave diffraction grating and a back-illuminated CCD camera, was used for recording the HHG spectra. A fiber spectrometer was employed for obtaining the fundamental beam's spectrum after the interaction with the gas. The fiber connected to the spectrometer collected the scattered IR light from the metallic filter (16 mm in diameter). This procedure allowed us to select the central part of the laser beam and to perform on-axis measurements. The HHG-yield optimization was done by adjusting the iris diameter, thus varying the laser energy on the target, $F_\#$, and consequently the IR laser pulse intensity at focus. Since the intensity gradient of the field is small in our loose-focusing geometry, we neglect contributions from Gouy phase shift Δk_G and atomic dipole phase Δk_d when we change the iris diameter. Besides, when we increase the laser driving intensity, the influence of the medium ionization on the phase-matching terms Δk_p and Δk_n becomes dominant. The optimal conditions were found to be $F_\# = 300$, $E = 50$ mJ for HHG in argon, the gas cell length and pressure were $L = 10$ cm and $p = 5$ mbar ($N_a = 1.25 \times 10^{23}$ atoms/m³), respectively. Here, the beam focus was at the center of the cell. On the other hand, for HHG in neon we have $F_\# = 240$, $E = 85$ mJ, $L = 4.4$ cm, and $p = 20$ mbar ($N_a = 5 \times 10^{23}$ atoms/m³). For this case the end of the gas cell was about 1.2 cm after the beam focus. Finally, $L = 3.6$ cm and the end of the gas cell was placed at the beam focus for HHG in helium. Here the optimal conditions were $F_\# = 200$, $E = 125$ mJ, and $p = 85$ mbar ($N_a = 2.13 \times 10^{24}$ atoms/m³).

Estimation of driving-laser intensity

The driving-laser intensity for different iris aperture sizes is estimated from the measured laser energy, pulse duration, and the focal spot intensity distribution. The intensity distribution of the attenuated beam is recorded directly by a CCD camera placed at the laser beam focus. On the other hand, the determination of the laser intensity I_{cutoff}, which one needs for generation of a high-order harmonic of energy $\hbar\omega_{\mathrm{cutoff}}$, is done by applying the semiclassical formula [21]

$$\hbar\omega_{\mathrm{cutoff}} = I_p + 3.17 U_p, \qquad (1)$$

where I_p is the ionization potential of the atom under consideration and U_p is the ponderomotive energy, which can be expressed as U_p [eV] $= 9.33 \times 10^{-14} I_{\mathrm{cutoff}}$ [W/cm²] λ_{IR}^2 [μm²], with λ_{IR} being the laser central wavelength. Finally, a particular estimated peak intensity is divided by a constant coefficient in order to get values closer to I_{cutoff}. The difference between the vacuum peak laser intensity and the I_{cutoff} mainly originates from the non-Gaussian temporal shape of the driving-laser pulse as well as aberrations of the focused beam. All the laser
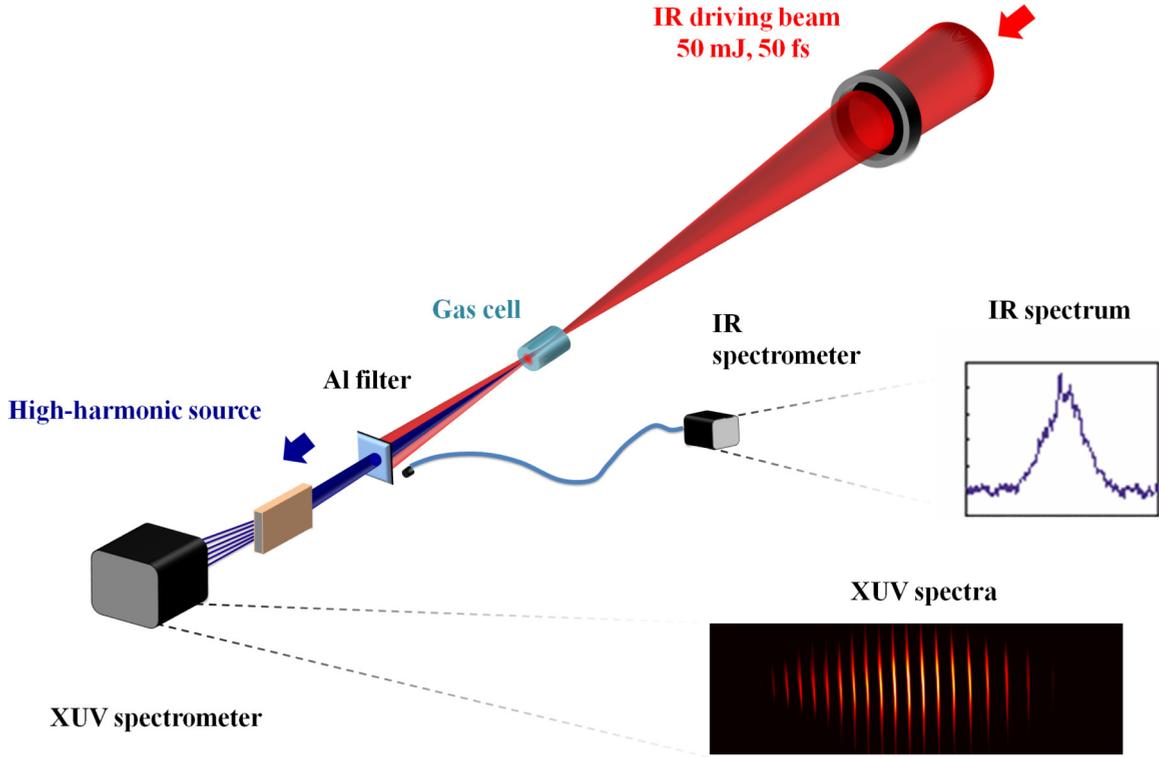
FIG. 1. Scheme of the experimental setup. By focusing an IR driving laser into a gas cell filled with rare gas, a harmonic beam is generated. An IR spectrometer records the driving-laser spectrum after the interaction with the gas and a XUV spectrometer detects the produced high-order harmonics spectra.

intensity values used in our calculations are computed with that coefficient kept constant.

III. THEORY

The harmonic phase originates from two components: one coming from the driving-laser field phase, defined as $\phi_{IR,q} = q\phi_{IR}$ [22,23], where ϕ_{IR} is the driving-laser phase and $\phi_{IR,q}$ is the phase of the qth harmonic, and another associated with the atomic dipole phase ϕ_{dipole}. Since the harmonics are generated by a laser pulse, the intensity of which varies in a temporal domain as $I(t)$, the dipole phase leads to frequency shift and chirp of the harmonic pulse. The resulting total phase of the generated harmonics $\phi_q(t)$ can then be written as

$$\phi_q(t) = \phi_{IR,q}(t) + \phi_{dipole}(t). \quad (2)$$

The instantaneous frequency of the qth harmonic is

$$\omega_{inst,q}(t) = \omega_q + \frac{\partial \phi_q(t)}{\partial t} = \omega_q + \Delta\omega_q(t)$$
$$= \omega_q + \Delta\omega_{IR,q}(t) + \Delta\omega_{dip}(t), \quad (3)$$

where $\Delta\omega_{IR,q}(t)$ and $\Delta\omega_{dip}(t)$ are frequency variations due to driving-laser frequency variation and atomic dipole contributions, respectively. The central wavelength shift can be expressed as $\Delta\lambda_q = \frac{\lambda_q^2}{2\pi c}\Delta\omega_q$. The contribution from the IR field, $\phi_{IR,q}$, will be treated in Sec. III A, while the contribution from the intrinsic dipole phase, ϕ_{dipole}, will be studied in Sec. III B.

A. Variation of driving-laser frequency

One can estimate the qth harmonic frequency, originating from the laser driving field $\phi_{IR,q}$ [see Eq. (2)], by considering plasma effects on the driving-laser pulse. The spectral shift $\Delta\omega_{IR}$ in the IR field due to plasma is transferred to a spectral shift $\Delta\omega_{p,q}$ of the qth harmonic via $\Delta\omega_{p,q} = q\Delta\omega_{IR}$ [22,23]. We compute the expected shift for the qth harmonic in two steps: first, only the shift of the driving laser is considered; second, the shift transferred to the harmonic field is estimated by taking into account the absorption in the medium. The laser pulse phase determined by modulation due to temporal variation of refractive index $n(t)$ after propagation through a medium of length L is

$$\phi_{IR}(t) = -\frac{2\pi}{\lambda_{IR}} \int_0^L n(t)dz, \quad (4)$$

leading to a plasma-induced frequency shift of

$$\Delta\omega_{IR}(t) = \frac{\partial \phi_{IR}(t)}{\partial t} = -\frac{2\pi}{\lambda_{IR}} \int_0^L \frac{\partial n(t)}{\partial t}dz, \quad (5)$$

where $n = \sqrt{1 + \chi_p + \chi_n}$ is the refractive index due to plasma and neutral atoms, and c is the speed of light. The electric susceptibility due to plasma is $\chi_p = -\frac{\omega_p^2}{\omega_0^2}$, where ω_p is the plasma frequency $\omega_p = (N_e e^2/\epsilon_0 m_e)^{1/2}$, with e being the elementary electric charge, ϵ_0 the vacuum permittivity, m_e the electron mass, and ω_0 the central angular frequency of the driving laser. The free-electron density is $N_e = \frac{\eta N_{atm} P}{p_0}$ with η being the ionization probability, N_{atm} the particle density

of an ideal gas at standard temperature and pressure (STP), $p_0 = 1$ atm, and p the actual gas cell pressure. Moreover, for neutral atoms one obtains $\chi_n = \frac{N_a e^2}{\epsilon_0 m_e (\omega_r^2 - \omega_0^2)}$ [24], where ω_r is the closest resonant frequency and the neutral atom density is given by $N_a = \frac{N_{\text{atm}} p (1 - \eta)}{p_0}$. Thus, both plasma and neutral atom contributions to the refractive index depend on the initial atomic density as well as on η.

It can be inferred from Eq. (5) that the spectral shift is proportional to (i) the medium length L, (ii) the ionization rate $\frac{\partial \eta}{\partial \tau}$, and (iii) the particle density N_a through the refractive index n. When the medium is strongly ionized, the plasma effect introduces a blueshift in the IR spectrum [25].

The main advantage of our study is the possibility to distinguish between the effect of the fundamental laser spectral shift and the effect coming from the intrinsic atomic dipole in the resulting high-harmonic spectral shift. This is possible, since we can determine the IR contribution by directly measuring its spectrum after propagation through the gas cell.

We measure the driving-laser spectra after the pulse propagates through the entire gas medium of length L. However, because high-order harmonics are generated from numerous positions throughout medium, it is important to estimate the effective contribution from the detected IR spectral shift to a resultant high-harmonic spectral shift. To take into account this fact, we apply a correction for calculation of $\Delta\lambda_{\text{IR}}$ to the resulting HHG spectral shift. For a simplified consideration, we assume a one-dimensional model and take into account that the IR laser acquires the spectral shift $\Delta\lambda_{\text{IR}}(z) = \frac{\Delta\lambda_{\text{IR}}}{L} z$. For high-order harmonics, the phase-matching conditions are fulfilled and the medium is considered homogeneous, the high-order harmonic signal develops along a medium of length L as [26]

$$I_q \propto \left| \left[\int_0^L E_q(z, \omega) \exp\left(-\frac{L - z}{2 L_{\text{abs}}} \right) \exp[i\phi_q(z)] dz \right] \right|^2, \quad (6)$$

where $E_q(z, \omega)$ is the amplitude of the atomic response around the harmonic frequency ω_q and $\phi_q(z)$ its phase, z is the distance along the propagation direction, and L_{abs} is the absorption length, defined as $L_{\text{abs}} = \frac{1}{\sigma N_a}$ (σ is the photoabsorption cross section). We estimate $L_{\text{abs}} = 10$ mm for argon, $L_{\text{abs}} = 3.7$ mm for neon, and $L_{\text{abs}} = 10.6$ mm for helium at the pressures given in Sec. II. Next, we need to evaluate the role of the emitters placed at different points in the medium considering that the shift of the IR, $\Delta\lambda_{\text{IR}}$, is acquired along the entire medium. We built up a simple model based on Eq. (6), assuming the harmonics are generated uniformly along the medium. Moreover, we assume that an emitter placed at a position z produces only monochromatic radiation corresponding to the actual laser frequency. Consequently, the spatial profile of the high-harmonic intensity, which is thus driven only by the exponential term, is directly imprinted in the spectrum. To be consistent with the experimental procedure for estimation of the central wavelength taking a median value, for the next analysis we consider the correction factor k given by the median of the profile as

$$k = 1 - \frac{2 L_{\text{abs}}}{L} \ln \left(\frac{2}{\exp\left(-\frac{L}{2 L_{\text{abs}}} \right) + 1} \right), \quad (7)$$

this value is already renormalized according to the transition from the spatial into the spectral domain. Finally, the effective high-harmonic spectral shift due to the laser wavelength shift reads $\Delta\lambda_{p,q} = k \Delta\lambda_{\text{IR}}/q$. With our experimental parameters we find that $k = 0.86$ for argon, $k = 0.88$ for neon, and $k = 0.72$ for helium.

B. Atomic dipole phase

The atomic dipole moment is the observable that is used to quantify the radiation generated by the qth harmonic at the single-emitter level. Its phase is determined by the Volkov classical action $S_V(t, t') = I_p(t - t') + \frac{1}{2} \int_{t'}^{t} [\mathbf{p} + \mathbf{A}(\tau)]^2 d\tau$ acquired by the laser-ionized free electron with drift momentum $\mathbf{p}$ at time t' oscillating in the driving-laser field until its recollision at time t, as $\phi_{\text{dipole}} = S_V(t, t') - q\omega_0 t$, i.e., by the value of the action along the most relevant semiclassical trajectory [21,27,28], where $\mathbf{A}(t) = -\int \mathbf{E}(t) dt$ is the laser's vector potential.

This phase is therefore governed by the time integral of the kinetic energy of the electron during its journey, which increases with the mean velocity, and therefore with the laser intensity.

The above explanation gives a straightforward physical picture of how the intrinsic dipole phase is acquired from a single emitter. In a simple approximation, the resulting phase shift is linear with intensity [29],

$$\phi_{\text{dipole}} = \phi_{\text{dipole}}(I) \approx -\alpha I + \text{const.,} \quad (8)$$

where the quantum-path phase coefficient $\alpha = \frac{\partial \phi_{\text{dipole}}}{\partial I}$ determines the core dependence of the harmonic phase on the laser intensity. It is characteristic for each generation regime, i.e., the long and short trajectories in plateau and the single trajectory in cutoff. The spectral shift can be also directly determined from a saddle-point calculation in the strong-field approximation (SFA). These are discussed in detail in Sec. IV C.

IV. RESULTS AND DISCUSSION

A. Phase matching

The major part of the XUV photon flux, during HHG, is produced provided that the phase-matching conditions are fulfilled. The medium refractive index n is strongly linked to the concentration of both free electrons, N_e, and neutral atoms, N_a, that in turn are dictated by the ionization probability η.

We use $\Delta k_q = \frac{q\omega_0}{c} \Delta n_{\text{pl,at}}$, where $\omega_0 = \frac{2\pi c}{\lambda_{\text{IR}}}$ and $\Delta n_{\text{pl,at}} = \Delta n_{\text{IR}} - \Delta n_q$, with Δn_{IR} and Δn_q being the refractive index variations due to plasma and neutral atoms for the driving laser and the qth-order harmonic, respectively. For estimation of the phase-matching ionization level we neglect variation of the refractive index of high-order harmonics, Δn_q, since it is significantly less than the variation of the refractive index of the driving laser, Δn_{IR}. The resulting phase-matching ionization level η_{PM} at which plasma and neutral-atom dispersion cancel each other [24] can be estimated as

$$\eta_{PM} \approx \left(1 + \frac{N_{\text{atm}} r_e \lambda_{\text{IR}}^2}{2\pi \Delta n} \right)^{-1}, \quad (9)$$
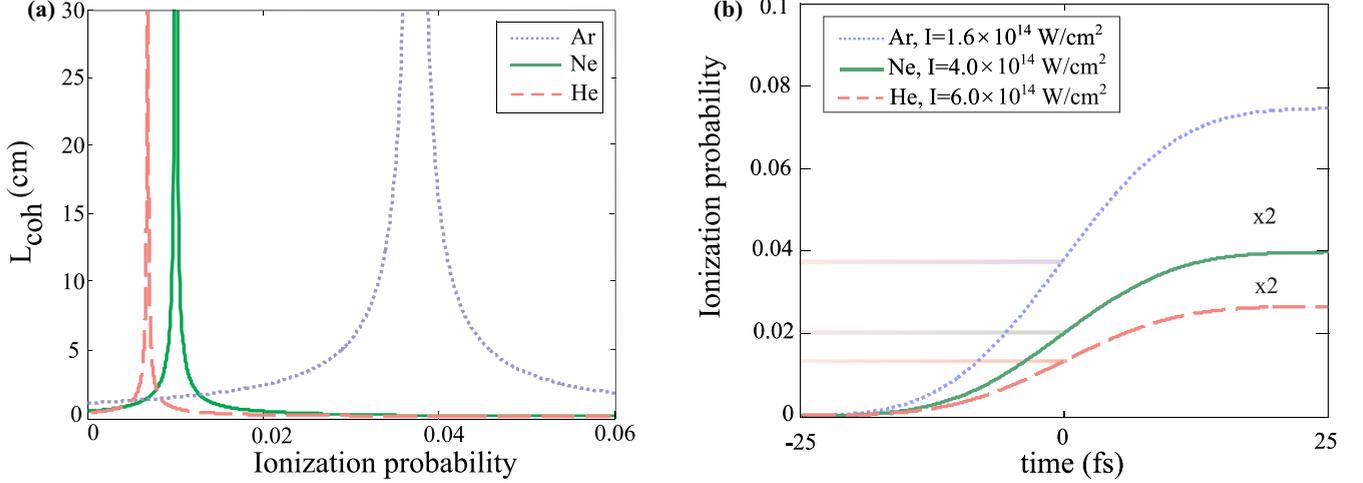
FIG. 2. (a) Coherence length L_{coh} as a function of η for the 25th harmonic generated in argon (blue dotted line); the 57th harmonic in neon (green solid line), and the 65th harmonic in helium (red dashed line). The calculation was done for particle densities, which corresponds to our experimental conditions (Sec. II). (b) Ionization probabilities η calculated for argon (blue dotted line), neon (green solid line), and helium (red dashed line). The horizontal lines define the phase-matched η values. The laser peak intensity values, $\hat{I}_{PM}$, where phase matching occurs at the peak of our 50 fs FWHM of intensity pulse, are provided in the legend.

where Δn is the change of the noble gas refractive index at one atmosphere of pressure, N_{atm} is the particle density of an ideal gas at STP conditions, and r_e is the classical electron radius.

We plot the coherence length L_{coh} as a function of η in Fig. 2(a), which was calculated for particle densities corresponding to our experimental conditions (Sec. II). As can be seen, there is an optimal value η_{PM} corresponding to ideal phase matching, of about ~3.8% for the 25th harmonic generated in argon with $\lambda_{IR} = 810$ nm, and about ~1.0% for the 57th harmonic in neon. Finally, we find that $\eta_{PM} \sim 0.66\%$ for the 65th harmonic generated in helium.

We can then define a laser intensity value, $\hat{I}_{PM}$, which corresponds to the generation of phase-matched high-order harmonics at the peak of the laser pulse. The static ionization rates in the tunneling and barrier-suppression regimes are computed by using the empirical formula from Ref. [30]. Figure 2(b) depicts the time dependence of η for HHG in argon, neon, and helium at different laser peak intensity values, $\hat{I}_{PM}$, for a 50 fs FWHM of intensity laser pulse with Gaussian distribution. The corresponding values of η_{PM} are indicated by colored horizontal lines.

B. Determination of intensity-dependent quantum-path phase coefficients

To determine the values of the quantum-path phase coefficient α, we calculate the harmonic dipole following the standard SFA formalism [21,27,28], in the form

$$\mathbf{D}(q\omega_0) = \sum_s d(t_{st}, t'_{st}) e^{-i S_V(t_{st}, t'_{st}) + i q \omega_0 t_{st}}, \quad (10)$$

where t_{st} and t'_{st} are the saddle-point solutions for recollision and ionization times at which the action $S_V(t, t') - q\omega_0 t$ is stationary, and we sum for a single-ionization burst over the first six quantum trajectories [31]. As can be seen, there are several return paths, which correspond to trajectories that

spend increasingly long times oscillating in the continuum before recombining with the ion. Note that some paths be closed at a given intensity for a fixed harmonic order, as the returning electron does not have enough energy to produce this particular harmonic. As the excursion time spent in the continuum increases, so does the phase coefficient α, so the first two returns (so-called short and long trajectories [28,31]) have the lowest values of α, with higher-order returns producing a more sensitive phase dependence on the intensity.

The phase of the emitted harmonics, then, is given by $\phi_{dipole} = \text{Re}(S_V(t_s, t'_s) - q\omega_0 t_s)$ and the α coefficient is obtained by numerical differentiation of this phase with respect to the intensity. The obtained α values as a function of laser intensity are shown in Fig. 3 for the 25th harmonic in argon [Fig. 3(a)], the 57th harmonic in neon [Fig. 3(b)], and the 65th harmonic in helium [Fig. 3(c)].

In our analysis we consider a piecewise dependence of α with the laser intensity and only the first two trajectories are relevant (one short and one long). We identify them according to the their respective recombination times t_1 and t_2.

C. Connection of atomic dipole spectral shift with intensity slope

We can predict the behavior of the expected spectral shift due to the atomic dipole phase. In the next analysis, we consider $\alpha(I)$, which provides a more accurate description of the phase variation according to Sec. IV B. The frequency variation due to the atomic dipole phase can be calculated by [27,32]

$$\Delta\omega_{dip}(t) = -\frac{\partial \phi_{dipole}(t)}{\partial t} = -\frac{\partial I}{\partial t}\left(\frac{\partial \alpha(I)}{\partial I}I + \alpha(I)\right). \quad (11)$$

First, we calculate the expected shift originating from the atomic dipole phase following the theory of Sec. III B and Eq. (11) with the α coefficients computed according to the procedure described in Sec. IV B. We assume that the high-order harmonic radiation is generated mostly in the temporal
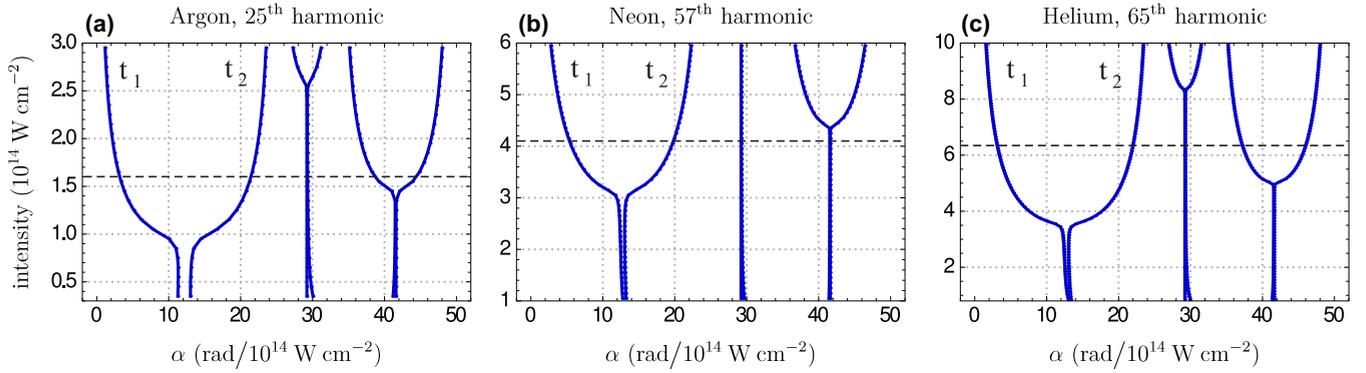
FIG. 3. Plot of the quantum-path phase coefficient α computed by using the SFA model for (a) the 25th harmonic in argon, (b) the 57th harmonic in neon, and (c) the 65th harmonic in helium. The horizontal black dashed lines indicate the intensity level $\hat{I}_{PM}$ at which phase-matching radiation is produced from the laser pulse peak.

region where the laser intensity provides an ionization degree η_{PM} corresponding to a phase-matching level (see Sec. IV A); we take the amount of frequency variation $\Delta\omega_{\text{dip}}$ due to the laser intensity slope at these points and calculate the expected wavelength shift as $\Delta\lambda_{\text{dip}} = \frac{\lambda_q^2}{2\pi c}\Delta\omega_{\text{dip}}$, where $\Delta\omega_{\text{dip}}$ is given by Eq. (11).

Figure 4 demonstrates calculated high-harmonic spectral shift due to the atomic dipole phase. Here, the short and long trajectories for the first return are considered. As can be inferred, α variation with intensity in Eq. (11) for a short trajectory leads to a noticeable blueshift at the low laser intensities (i.e., in conditions where $I_{\text{peak}} < \hat{I}_{PM}$) and minor and slowly varying redshift at high laser intensities ($I_{\text{peak}} > \hat{I}_{PM}$). In contrast, spectral shift due to the atomic dipole, taking into account a long electron trajectory predicts visible redshift at the low laser intensities ($I_{\text{peak}} < \hat{I}_{PM}$) and strong blueshift at high intensities ($I_{\text{peak}} > \hat{I}_{PM}$). These data will assist in the identification of the dominant electron trajectory during experiment, as can be seen in next section.

D. Measured and calculated spectral shifts

We study the intensity-dependent central-wavelength shift of both the driving laser and particular high-order harmonics. To identify the origin of the high-order harmonic spectral shift following Eq. (3), both the frequency shift due to the atomic dipole as well as the spectral shift of the driving IR laser contribution should be taken into account. The predicted wavelength shifts due to the atomic dipole phase are shown in Fig. 4 for argon, neon, and helium atoms.

For the determination of the IR spectral shift, $\Delta\lambda_{\text{IR}}$, we use the recorded laser pulse spectra. This allows us to separate out the effect of the IR laser wavelength shift due to plasma in the resulting high-order harmonic wavelength shift. The driving pulse spectral shifts after the laser-target interaction during HHG in argon, neon, and helium are shown in Figs. 5(a)–5(c), respectively. Besides, the high-order harmonic spectral shifts for the 25th harmonic in argon, the 57th in neon, and the 65th in helium are also demonstrated. The spectral shift of the IR is defined as the difference between the central wavelength, obtained as the median value of the spectral intensity distribution of the incoming driving IR laser field, and the one

after the interaction with the gas target. A similar procedure is employed for the calculation of the high-order-harmonic wavelength shift.

To figure out which electron trajectory dominates the generation process in our experimental conditions, we calculate the expected high-order harmonic spectral shift, taking into account the atomic dipole phase according to Eq. (2) for each kind of electron trajectory. In this way, we are able to identify the contributions coming from the long and short trajectories based on the obtained experimental data. We thus calculate the resulting high-order harmonic spectral shift in wavelength as

$$\Delta\lambda_q = a\Delta\lambda_{\text{dip},t_1} + (1-a)\Delta\lambda_{\text{dip},t_2} + k\frac{\Delta\lambda_{\text{IR}}}{q}. \quad (12)$$

The a factor accounts for the short electron trajectory contribution fraction. To find it, we consider values $\Delta\lambda_q$ (measured high-harmonic spectral shift), $\Delta\lambda_{\text{IR}}$ (measured driving-laser spectral shift), k [correction factor according to Eq. (7)], and q (harmonic order) to solve Eq. (12) for each peak-intensity point. Since the term $-\frac{\partial I}{\partial t}$ in Eq. (11) leads to zero spectral shift, when the phase-matched harmonic generation is produced at the peak of the pulse, it is therefore impossible to determine a for these intensity values.

Taking into account that our XUV spectrometer is not calibrated in absolute terms, we set the zero shift at the peak intensities $\hat{I}_{PM}$ for all cases (indicated as vertical black dashed lines in the figures).

At low peak intensities, the laser intensity is not enough to reach an ionization level suitable for phase matching η_{PM}. Thus, we cannot apply Eq. (12) to determine a from experimentally measured data. The high-order harmonics of interest are produced near cutoff at low peak intensities. The α values are known for these intensity values, as can be seen in Fig. 3. Therefore, it becomes possible to use the measured high-harmonic spectral shift to determine at which intensity (and corresponding time) the dominating harmonic generation takes place.

We study the correlation of the driving IR laser wavelength shift and that of the 25th harmonic order in argon as a function of driving-laser intensity, as illustrated in Fig. 5(a). As can be seen, the obtained high-order harmonic spectral shift $q\Delta\lambda_q$ is predominantly given by the shift $\Delta\lambda_{\text{IR}}$ of the fundamental
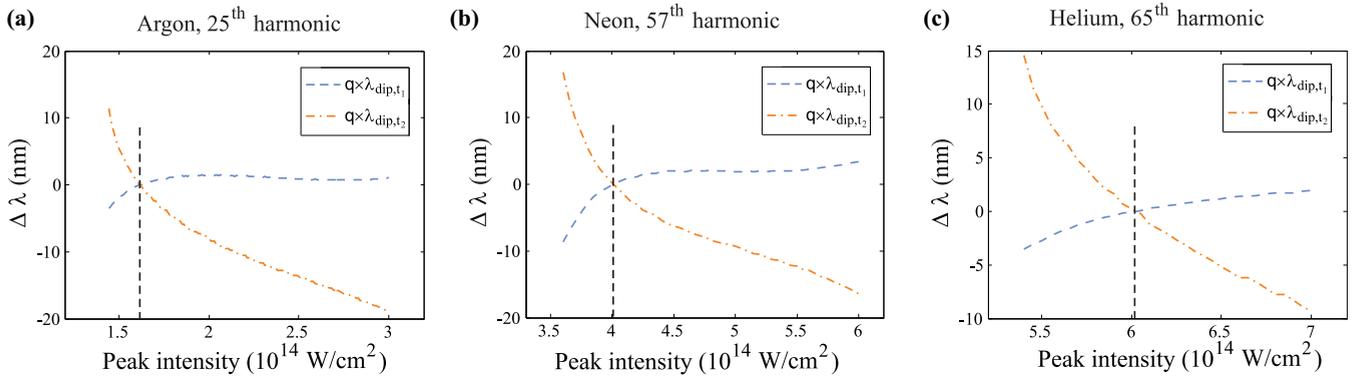
FIG. 4. Spectral wavelength shift due to atomic dipole phase calculated according to Eq. (11) for HHG produced in phase-matching time for (a) argon, (b) neon, and (c) helium. The α values are taken from Fig. 3. The dashed black lines correspond to the intensity level $\hat{I}_{PM}$ at which phase-matching radiation is produced from the laser pulse peak.

laser wavelength. Even though the uncertainty is high, the a factor is found to be $a \approx 0.9$, implying that a short electron trajectory dominated the process. Thus, the spectral shift induced by the atomic dipole phase is minor for this case and the high-harmonic spectral shift follows that of the driving laser. Such behavior is consistent with that reported in the literature [22,33].

Next, we consider the spectral shift of the driving-laser wavelength and that of the 57th harmonic order in neon, which is shown in Fig. 5(b). Based on the data obtained, by separating the effect of the IR spectral shift, we find that the contribution coming from the atomic dipole phase introduces a redshift at laser peak intensities less than $\hat{I}_{PM}$. At such low laser intensities, plasma does not significantly influence the driving-laser pulse. Thus its contribution to the wavelength shift is negligible. As a consequence, we conclude that the spectral shift induced by the atomic dipole phase is responsible for the observed high-harmonic spectral shift. The fraction of the short electron trajectory is found to be $a \approx 0.7$ for HHG in neon. Higher relevance of the long electron path can be caused by the gas target being before the laser beam focus, since this position assists phase matching of the HHG with the predominance of the long electron trajectory [20,34,35].

Furthermore, we investigate the correlation between the IR laser wavelength shift and that of the 65th harmonic order in helium, as demonstrated in Fig. 5(c). A large high-order harmonic redshift $q \Delta\lambda_q$ is observed while $\Delta\lambda_{\text{IR}}$ is negligible, before the gas medium becomes significantly ionized. Consequently, for this case we conclude that the contribution from the atomic dipole phase is dominant for the same reason as for the case of HHG in neon. The fraction of the short electron trajectory is found to be $a \approx 0.75$ for HHG in helium.

During HHG in all cases, the origin of the harmonic spectral shift for lowest peak intensities was studied. It was found that cutoff harmonics are mainly generated in the trailing part of the laser pulse peak close to its apex.

E. Spectral broadening of high-order harmonics

We studied the spectral broadening of high-order harmonics as a function of laser intensity. The harmonic spectral width Δ_q is inversely proportional to the high-harmonic pulse duration $\Delta\tau_q$ (the FWHM of the qth-order harmonic intensity), where $\Delta_q \propto \frac{1}{\Delta\tau_q}$.

For our analysis we assume that the harmonic pulse duration is equal to the time interval, where the phase-matched
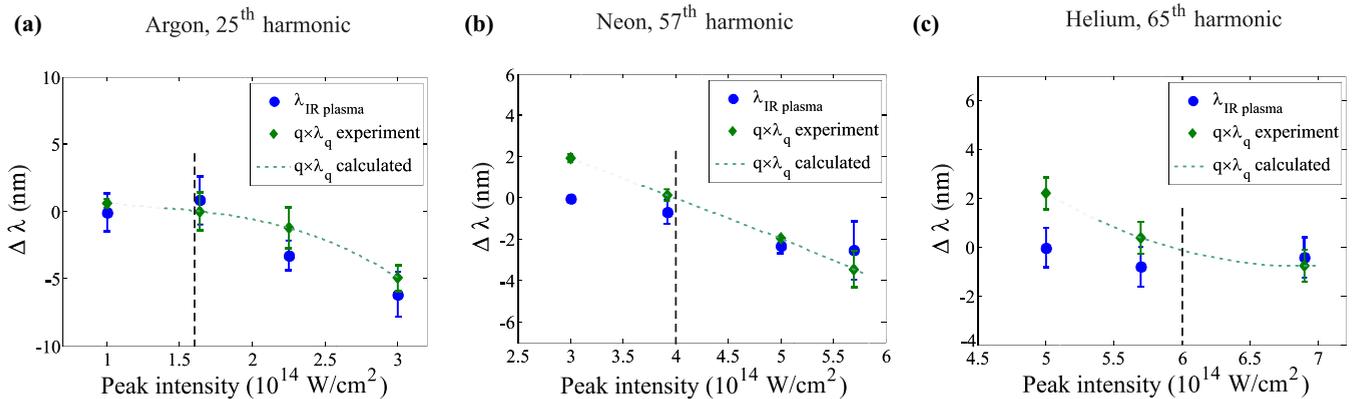
FIG. 5. Comparison between the experimentally measured high-order harmonic spectral shifts (green diamonds), driving laser spectral shifts (blue circles), and calculated values (light green dashed curve) of expected high-order-harmonic shifts in accordance with Eq. (12) for harmonic orders 25th, 57th, and 65th generated in (a) argon, (b) neon, and (c) helium gases, respectively. Vertical dashed black lines indicate the intensity level $\hat{I}_{PM}$ at which phase-matching radiation is produced from the laser pulse peak.
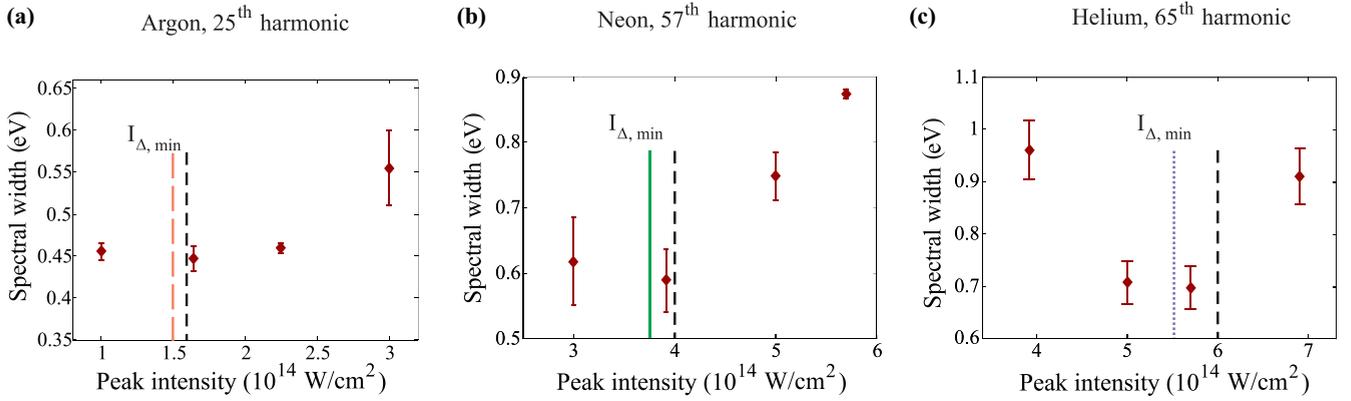
FIG. 6. Comparison between the experimentally measured high-order harmonic spectral broadening as a function of the driving laser intensity (red solid diamonds). The presented data are for the 25th, 57th, and 65th harmonic orders generated in (a) argon, (b) neon, and (c) helium, respectively. The vertical (a) long dashed, (b) solid, and (c) dotted lines correspond to the $I_{\Delta,\min}$ values (see text for details). The dashed black lines indicate the intensity levels $\hat{I}_{PM}$.

generation occurs, as described below. First we estimate from the optimal generation conditions the time intervals where we reach an η suitable for phase matching. To do this, we first obtain the η dependence of the length-density product, which is defined as $L_{\mathrm{coh}} N_a$. Combining the calculated $L_{\mathrm{coh}} N_a$ and the experimentally estimated LN_a products, we find the phase-matching ionization degree ranges $[\eta_{\min}, \eta_{\max}]$ under our optimal experimental conditions. We thus obtain a range between 2.8% to 4.2% for the 25th harmonic generated in argon, from 0.89% to 1.1% for the $q = 57$th harmonic generated in neon, and from 0.63% to 0.7% for the $q = 65$th harmonic order in the case of helium gas. Defining respective phase-matching times $\tau_{PM,1}$ and $\tau_{PM,2}$ for the lower and upper limits of the phase-matching ionization ranges, the corresponding phase-matching time interval $T_{PM} \equiv [\tau_{PM,1}, \tau_{PM,2}]$ and varies with the laser peak intensity.

We introduce an additional assumption, which takes into account the limitation arising from the single-atom response of the HHG process. This implies that the HHG occurs within a laser intensity region, where the intensity is large enough to produce harmonics above cutoff, i.e., $I > I_{\mathrm{cutoff}}$. The determination of the laser intensity I_{cutoff} needed for the generation of a high-order harmonic of energy $\hbar\omega_{\mathrm{cutoff}}$ is done by invoking the semiclassical formula (1) [21]. We can then define a time interval which corresponds to an intensity range fulfilling the condition $I > I_{\mathrm{cutoff}}$. This condition defines the times $\tau_{\mathrm{cutoff},1}$ and $\tau_{\mathrm{cutoff},2}$ and consequently we find $T_{\mathrm{cutoff}} \equiv [\tau_{\mathrm{cutoff},1}, \tau_{\mathrm{cutoff},2}]$.

We now apply both conditions for each particular laser peak intensity and search for the intersection between the time intervals T_{PM} and T_{cutoff}, so that the final time interval is then $T_q \equiv T_{PM} \cap T_{\mathrm{cutoff}}$. At low laser peak intensities, T_{PM} is very large. This happens because the upper boundary of the phase-matching ionization level is not reached. The total high-order harmonic pulse duration T_q is therefore limited by $\tau_{PM,1}$ and $\tau_{\mathrm{cutoff},2}$. The longest T_q is achieved when $\tau_{PM,2} = \tau_{\mathrm{cutoff},2}$. As the laser peak intensity increases, the upper level of the phase-matching ionization degree is reached and the duration T_q is fully given by T_{PM}, since $T_{PM} \subseteq T_{\mathrm{cutoff}}$. Thus, the time interval T_q shortens as the laser peak intensity rises. This

reduction is caused by the sudden growth of the ionization probability. Following these precepts, we can define the minimal high-order harmonic spectral width, which corresponds to a maximum T_q as $\Delta_{q,\min}$. The laser peak intensity at which this value is reached is then defined as $I_{\Delta,\min}$.

We demonstrate the experimentally measured dependence of the high-order harmonic spectral width on the increase of the driving-laser intensity in Fig. 6 for the 25th harmonic order in argon [Fig. 6(a)], the 57th in neon [Fig. 6(b)], and the 65th in helium [Fig. 6(c)]. The values $I_{\Delta,\min}$ were found to be 1.5×10^{14}, 3.74×10^{14}, and 5.5×10^{14} W/cm^2 for the particular harmonics generated in argon, neon, and helium, respectively. As can be seen, the experimentally measured high-order harmonic spectral width shows a minimum around the calculated $I_{\Delta,\min}$ values. We thus attribute this spectral width minimum to the maximum high-order harmonic pulse duration T_q, obtained by considering that the laser intensity is limited, on the one side, by the HHG cutoff and by the phase-matching conditions on the other side.

We have also studied the influence of the chirp due to the time-dependent high-order harmonic phase variation, on the high-order harmonic spectral broadening in accordance with assumptions from Refs. [32,36]. For this calculation we take into account the intensity values in those time intervals, which is when phase-matched HHG occurs. Taking into account both effects, i.e., the variation of T_q as well as the high-order harmonic chirp due to the atomic dipole phase, we find that the actual effect of the latter is much weaker than the variation of the high-order harmonic pulse duration. Including the chirp contribution in our analysis, its effect is observed only close to regions with the smallest spectral width, i.e., close to $\hat{I}_{PM}$, since the second derivative of intensity with respect to time is largest here. In this way, the obtained spectral broadening increases by about 4% of the maximal spectral width. Thus, it may be assumed to be negligible under our conditions.

V. CONCLUSIONS

In conclusion, we performed a comprehensive study of the HHG spectral features in noble gases with different ionization

potentials. The ability to measure the driving laser's spectral shift makes it possible to disentangle the different contributions to the resulting high-order harmonic wavelength shift. In this way, we can distinguish the wavelength shift coming directly from the driving IR laser pulse from that produced by the atomic dipole phase. We found the contribution to the resultant high-harmonic spectral shift due to the atomic dipole phase in the case of HHG in argon is negligible. On the other hand, this contribution is non-negligible in our experiment in the cases of neon and helium. The relative contributions for our experimental conditions coming from long and short electron trajectories were determined by using measured driving-laser and high-harmonic spectral shifts as well as a computed intensity-dependent α coefficient. Our main observations lead to the conclusion that the spectral shift of high-order harmonics corresponds to a shift in the driving-laser spectra only when the contributions of the long and short trajectory compensate each other, providing negligible spectral shift due to the atomic dipole phase. This is the case as long as the contribution of a long trajectory is quite small, about 10%. Otherwise, the spectral shift due to the atomic dipole phase is not negligible and the resulting high-harmonic shift does not follow that of the driving laser. This conclusion is of high importance for experiments, where exact knowledge of the spectral position of high-order harmonics is of instrumental relevance.

Additionally, we studied the spectral broadening of the high-order harmonics generated in different gases. The smallest spectral width was determined at the laser peak intensity that provides the largest time intersection between the microscopic assumptions, when the laser intensity exceeds the cutoff value, and the macroscopic assumptions, when the phase-matching ionization level is achieved. For all atomic species, the narrowest high-order harmonic width was localized at laser peak intensities lower than that corresponding to phase-matching radiation from the peak of the pulse (when the medium is not over-ionized). The influence of the atomic dipole chirp on the high-order harmonic spectral broadening was found to be negligible in our study.

The data presented and its analysis provide a significant extension of the knowledge of HHG spectral characteristics.

[1] F. Krausz and M. Y. Ivanov, Attosecond physics, Rev. Mod. Phys. **81**, 163 (2009).

[2] T. Ditmire, E. T. Gumbrell, R. A. Smith, J. W. G. Tisch, D. D. Meyerhofer, and M. H. R. Hutchinson, Spatial Coherence Measurement of Soft X-Ray Radiation Produced by High Order Harmonic Generation, Phys. Rev. Lett. **77**, 4756 (1996).

[3] J. Gautier, P. Zeitoun, C. Hauri, A.-S. Morlens, G. Rey, C. Valentin, E. Papalarazou, J.-P. Goddet, S. Sebban, F. Burgy, P. Mercère, M. Idir, G. Dovillaire, X. Levecq, S. Bucourt, M. Fajardo, H. Merdji, and J.-P. Caumes, Optimization of the wave front of high-order harmonics, Eur. Phys. J. D **48**, 459 (2008).

[4] A. Fleischer, O. Kfier, T. Diskin, and P. Sidorenko, Spin angular momentum and tunable polarization in high-harmonic generation, Nat. Photonics **8**, 543 (2014).

[5] N. Zhavoronkov and M. Ivanov, Extended ellipticity control for attosecond pulses by high harmonic generation, Opt. Lett. **42**, 4720 (2017).

[6] E. J. Takahashi, T. Kanai, K. L. Ishikawa, Y. Nabekawa, and K. Midorikawa, Dramatic Enhancement of High-Order Harmonic Generation, Phys. Rev. Lett. **99**, 053904 (2007).

[7] P. Paul, E. Toma, P. Breger, G. Mullot, F. Auge, Ph. Balcou, H. Muller, and P. Agostini, Observation of a train of attosecond pulses from high harmonic generation, Science **292**, 1689 (2001).

[8] J. Li, X. Ren, Y. Yin, K. Zhao, A. Chew, Y. Cheng, E. Cunningham, Y. Wang, S. Hu, Y. Wu, M. Chini, and Z. Chang, 53-attosecond X-ray pulses reach the carbon K-edge, Nat. Commun. **8**, 186 (2017).

[9] P. B. Corkum and F. Krausz, Attosecond science, Nat. Phys. **3**, 381 (2007).

[10] M. Uiberacker, Th. Uphues, M. Schultze, A. J. Verhoef, V. Yakovlev, M. F. Kling, J. Rauschenberger, N. M. Kabachnik, H. Schröder, M. Lezius, K. L. Kompa, H.-G. Muller, M. J. J. Vrakking, S. Hendel, U. Kleineberg, U. Heinzmann, M. Drescher, and F. Krausz, Attosecond real-time observation of electron tunneling in atoms, Nature (London) **446**, 627 (2007).

[11] B. Vodungbo, J. Gautier, G. Lambert, A. Barszczak Sardinha, M. Lozano, S. Sebban, M. Ducousso, W. Boutu, K. Li, B. Tudu, M. Tortarolo, R. Hawaldar, R. Delaunay, V. López-Flores, J. Arabski, C. Boeglin, H. Merdji, Ph. Zeitoun, and J. Lüning,

Laser-induced ultrafast demagnetization in the presence of a nanoscale magnetic domain network, Nat. Commun. **3**, 999 (2012).

[12] X. Zhou, R. Lock, W. Li, N. Wagner, M. M. Murnane, and H. C. Kapteyn, Molecular Recollision Interferometry in High Harmonic Generation, Phys. Rev. Lett. **100**, 073902 (2008).

[13] P. Tzallas, E. Skantzakis, L. A. A. Nikolopoulos, G. D. Tsakiris, and D. Charalambidis, Extreme-ultraviolet pump-probe studies of one-femtosecond-scale electron dynamics, Nat. Phys. **7**, 781 (2011).

[14] B. Manschwetus, L. Rading, F. Campi, S. Maclot, H. Coudert-Alteirac, J. Lahl, H. Wikmark, P. Rudawski, C. M. Heyl, B. Farkas, T. Mohamed, A. L'Huillier, and P. Johnsson, Two-photon double ionization of neon using an intense attosecond pulse train, Phys. Rev. A **93**, 061402(R) (2016).

[15] P. B. Corkum, Plasma Perspective on Strong Field Multiphoton Ionization, Phys. Rev. Lett. **71**, 1994 (1993).

[16] K. C. Kulander, K. J. Schafer, and K. L. Krause, Super-Intense Laser–Atom Physics, in *Vol. 316 of NATO Advanced Study Institute Series B: Physics*, edited by B. Piraux, A. L'Huillier, and K. Rzazewski (Plenum, New York, 1993), p. 95.

[17] J. L. Krause, K. J. Schafer, and K. C. Kulander, High-Order Harmonic Generation from Atoms and Ions in the High Intensity Regime, Phys. Rev. Lett. **68**, 3535 (1992).

[18] T. Ruchon, C. P. Hauri, K. Varjú, E. Gustafsson, R. López-Martens, and A. L'Huillier, Macroscopic effects in attosecond pulse generation, New J. Phys. **10**, 025027 (2008).

[19] C. Delfin, C. Altucci, F. De Filippo, C. de Lisio, M. B. Gaarde, A. L'Huillier, L. Roos, and C.-G. Wahlström, Influence of the medium length on high-order harmonic generation, J. Phys. B: At., Mol. Opt. Phys. **32**, 5397 (1999).

[20] H. Merdji, M. Kovačcev, W. Boutu, P. Salières, F. Vernay, and B. Carré, Macroscopic control of high-order harmonics quantum-path components for the generation of attosecond pulses, Phys. Rev. A **74**, 043804 (2006).

[21] M. Lewenstein, Ph. Balcou, M. Y. Ivanov, A. L'Huillier, and P. B. Corkum, Theory of high-harmonic generation by low-frequency laser fields, Phys. Rev. A **49**, 2117 (1994).

[22] C.-G. Wahlström, J. Larsson, A. Persson, T. Starczewski, S. Svanberg, P. Salières, Ph. Balcou, and A. L'Huillier, High-order harmonic generation in rare gases with an intense short-pulse laser, Phys. Rev. A **48**, 4709 (1993).

[23] S. C. Rae and K. Burnett, Harmonic generation and phase matching in the tunneling limit, J. Phys. B: At., Mol. Opt. Phys. **26**, 1509 (1993).

[24] Z. Chang, *Fundamentals of Attosecond Optics* (CRC Press, Boca Raton, 2011).

[25] S. P. Le Blanc, R. Sauerbrey, S. C. Rae, and K. Burnett, Spectral blue shifting of a femtosecond laser pulse propagating through a high-pressure gas, J. Opt. Soc. Am. B **10**, 1801 (1993).

[26] E. Constant, D. Garzella, P. Breger, E. Mével, C. Dorrer, C. Le Blanc, F. Salin, and P. Agostini, Optimizing High Harmonic Generation in Absorbing Gases: Model and Experiment, Phys. Rev. Lett. **82**, 1668 (1999).

[27] M. Lewenstein, P. Salières, and A. L'Huillier, Phase of the atomic polarization in high-order harmonic generation, Phys. Rev. A **52**, 4747 (1995).

[28] M. Ivanov and O. Smirnova, Multielectron High Harmonic Generation: simple man on a complex plane, in *Attosecond and XUV Physics: Ultrafast Dynamics and Spectroscopy*, edited by T. Schultz and M. Vrakking (Wiley-VCH, Weinheim, 2014), pp. 201–256.

[29] F. Catoire, A. Ferré, O. Hort, A. Dubrouil, L. Quintard, D. Descamps, S. Petit, F. Burgy, E. Mável, Y. Mairesse, and E. Constant, Complex structure of spatially resolved high-order-harmonic spectra, Phys. Rev. A **94**, 063401 (2016).

[30] X. M. Tong and C. D. Lin, Empirical formula for static field ionization rates of atoms and molecules by lasers in the barrier-suppression regime, J. Phys. B: At., Mol. Opt. Phys. **38**, 2593 (2005).

[31] D. B. Milošević and W. Becker, Role of long quantum orbits in high-order harmonic generation, Phys. Rev. A **66**, 063417 (2002).

[32] M. Murakami, J. Mauritsson, and M. B. Gaarde, Frequency-chirp rates of harmonics driven by a few-cycle pulse, Phys. Rev. A **72**, 023413 (2005).

[33] C. Kan, C. E. Capjack, R. Rankin, and N. H. Burnett, Spectral and temporal structure in high harmonic emission from ionizing atomic gases, Phys. Rev. A **52**, R4336(R) (1995).

[34] P. Balcou, P. Salières, A. L'Huillier, and M. Lewenstein, Generalized phase-matching conditions for high harmonics: The role of field-gradient forces, Phys. Rev. A **55**, 3204 (1997).

[35] L. E. Chipperfield, P. L. Knight, J. W. G. Tisch, and J. P. Marangos, Tracking individual electron trajectories in a high harmonic spectrum, Opt. Commun. **264**, 494 (2006).

[36] Z. Chang, A. Rundquist, H. Wang, I. Christov, H. C. Kapteyn, and M. M. Murnane, Temporal phase control of soft-x-ray harmonic emission, Phys. Rev. A **58**, R30(R) (1998).